AD-A221 935

OFFICE OF NAVAL RESEARCH

Grant N00014-90-J-1235

R & T Code 4133020

Technical Report No. 2

Infrared Reflection-Absorption Sepctroscopy of the Electrode/Electrolyte Solution Interface: Optical Considerations

by

Peter W. Faguy and W. Ronald Fawcett

Prepared for Publication

in

Applied Spectroscopy

DTIC
ELECTE
MAY 29 1990
S B D

Department of Chemistry
University of California
Davis, CA 95616

May 1, 1990

Reproduction in whole or in part is permitted
for any purpose of the United States Government

"This document has been approved for public release
and sale; its distribution is unlimited"

REPORT DOCUMENTATION PAGE	1. REPORT NO.	2.	3. Recipient's Accession No.
4. Title and Subtitle: Infrared Reflection-Absorption Spectroscopy of the Electrode/Electrolyte Solution Interface: Optical Considerations			5. Report Date: May 1, 1990 6.
7. Author(s): Peter W. Faguy and W.Ronald Fawcett			8. Performing Organization Rept. No.
9. Performing Organization Name and Address: Department of Chemistry University of California Davis, CA 95616			10. Project/Task/Work Unit No. 11. Contract(C) or Grant(G) No. (C) N00014-90-J-1235 (G)
12. Sponsoring Organization Name and Address: Office of Naval Research 800 N. Quincy Arlington, VA 22217-5000			13. Type of Report & Period Covered: Technical 14.
15. Supplementary Notes: Prepared for publication in Applied Spectroscopy			

16. Abstract (Limit: 200 words)

Calculations based on the classical Fresnel equations have been carried out to investigate the effect of various experimental parameters on infrared spectra obtained for molecules adsorbed at the electrode/solution interface. The effects considered include the nature of window material, variation in the angle of incidence, incident beam diameter, instrument focus, and the presence of an absorbing bulk electrolyte solution. It is shown that under certain circumstances, the resultant spectra are enhanced with respect to those obtained in the absence of an IR window and bulk absorbing phase. The significance of the present results with respect to practical experiments is discussed.

17. Document Analysis a. Descriptors

Electrochemistry, Physical Optics, Reflection Spectroscopy, EMIRS, SNIFTIRS, IRRAS (JG)

b. Identifiers/Open-Ended Terms

c. COSATI Field/Group

18. Availability Statement	19. Security Class (This Report): Unclassified	21. No. of Pages
	20. Security Class (This Page)	22. Price

(See ANSI-Z39.18) See Instructions on Reverse OPTIONAL FORM 272 (4-77)

* 291 : 1993 0 - 301-526 (8393)

Infrared Reflection-Absorption Spectroscopy of the Electrode/Electrolyte Interface: Optical Considerations

Peter W. Faguy and W. Ronald Fawcett

Department of Chemistry

University of California, Davis

Davis, CA 95616

ABSTRACT

Calculations based on the classical Fresnel equations have been carried out to investigate the effect of various experimental parameters on infrared spectra obtained for molecules adsorbed at the electrode/solution interface. The effects considered include the nature of window material, variation in the angle of incidence, incident beam diameter, instrument focus, and the presence of an absorbing bulk electrolyte solution. It is shown that under certain circumstances, the resultant spectra are enhanced with respect to those obtained in the absence of an IR window and bulk absorbing phase. The significance of the present results with respect to practical experiments is discussed.

INDEX HEADINGS

Electrochemistry, physical optics, reflection spectroscopy

Accession For	
NTIS GRA&I	☑
DTIC TAB	☐
Unannounced	☐
Justification	
By	
Distribution/	
Availability Codes	
Dist	Avail and/or Special
A-1	

INTRODUCTION

In recent years infrared spectroscopic techniques such as EMIRS (electrochemically modulated infrared spectroscopy) and SNIFTIRS (subtractively normalized interfacial Fourier transform infrared spectroscopy) have become the pre-eminent means of probing molecular structure at the electrode-electrolyte solution interface.[1,2] One of the most important advantages of these infrared reflection-absorption spectroscopic (IRRAS) measurements is that the physical optics involved is interpretable in terms of classical electromagnetic field theory. The propagation, reflection and attenuation of infrared light in the spectroelectrochemical cell can be described using the appropriate boundary conditions and Maxwell's equations. Simulation of the IRRA spectra can be used to better determine the optical constraints in an *in situ* experiment. In the present work, classical physical optics is used to model the IR spectrum of adsorbed solvent molecules in the presence of a bulk solvent layer, with the aim of gaining the necessary information to optimize the IR spectroelectrochemical measurement.

Since the chemical species of interest are confined to a monolayer, the *in situ* IRRAS experiment may require the reproducible measurement of relative intensity changes as small as 1 part in 10^5. The presence of an IR window and the bulk electrolyte solution in the optical path, before and after the electrode surface, effects the overall intensity reaching the detector by attenuation and by possibly introducing dispersion- distortion effects due to the complex refractive indices of the layers traversed.[3] Measuring the IR spectra of an adsorbed solvent layer is made even more difficult by the presence of the bulk solvent bands only a few wavenumbers removed from the analogous bands due to the interfacial species. This means that the IR radiation available for absorption by the adsorbed solvent is severely attenuated by the nearby bulk solvent band and that bulk solvent anomalous dispersion effects might influence the final spectrum observed.

Several papers have appeared in the literature using Fresnel formulae to calculate mean electric field strengths and reflectivities for different spectroelectrochemical configurations.[4-7] Seki *et al.*[4] have discussed the effect of an aqueous bulk electrolyte layer on the polarization

modulation differential reflectance (PMDR) spectrum. They consider the effect of water layer thickness both on the PMDR spectrum and on the mean square electric field strength in the aqueous layer. The mean electric field strength responsible for the enhanced infrared absorption of adsorbed species in a Kretschmann attenuated total reflection (ATR) configuration has been modelled by Osawa *et al.*[5] Other workers[6,7] have described the physical optics of a three layer spectroelectrochemical cell in which the effects of the metal electrode, the adsorbed layer, the bulk electrolyte, and the IR transparent window are considered.

The purpose of the present work is to use theoretical calculations based on physical optics to identify optimum optical configurations for the SNIFTIRS or EMIRS experiment and to determine which parameters influence the signal intensity and the signal-to-noise ratio (SNR) of the *in situ* measurement.

REFLECTIVITY CALCULATIONS

The effect of focussed optics,the bulk electrolyte layer, and different window materials and geometries are quantitatively developed in the following using simulated normalized reflectivities. The normalized difference reflectivity ($-\Delta R/R$) spectra are calculated from classical physical optics for the transmission and reflection of IR light through layered media.[8-10] The thin-layer cell is modelled as a series of layers each with distinct optical constants assuming that the media are isotropic, homogeneous and linear. Depending on the particular system modelled, from two to five layers are used to calculate the reflectivity. Figure 1 shows a generalized schematic diagram of the thin-layer cell where θ_1 is the incident angle, d_2 is the thickness of the second layer and n_{N-1} is the complex, frequency dependent, refractive index of the adsorbed layer. The actual calculations were performed using FORTRAN routines[11] run on an 80286 based personal computer and formulated from the characteristic matrix description for stratified optical media.[12] All $-\Delta R/R$ spectra are calculated from a reference reflectivity (R_r) and a sample reflectivity (R_s) for radiation polarized parallel to the plane of incidence according to the following equation,

$$-\Delta R/R(\nu) = -(R_s-R_r)/R_r = 1 - R_s/R_r \qquad [1]$$

where the sample system contains the adsorbate layer and the reference system does not. Potential dependent effects such as band and intensity shifts and concentration changes in the diffuse layer have not been included.

In some cases, noise was added to the simulated reflectivities as 7 bits of digital uncertainty on 24 bits of signal; this is equivalent to an analog gain of 2 before filling the analog-to-digital converter each scan and then signal averaging 1024 times. This hypothetical signal level is optimistic; in real experimental configurations, much less intensity may reach the detector. The purpose of the digital noise is to identify limiting signal cases. In these simulated spectra the regions of poorest SNR can be identified with the limiting regions in real experiments.

Where necessary, the effect of a broad band source and commercial spectrometer optics was approximated by a distribution of incident angles and by an attenuation factor for the projection of the beam image on the sample plane. The reflectivities calculated for a single angle of incidence (θ_1) are replaced by a weighted average over the angular divergence. Gaussian coefficients were used and the beam spread was set at ±6°. The attenuation factor, A, is given by the following equation,

$$A = 1 \qquad \text{for } \alpha \geq 1$$

$$\text{and} \qquad [2]$$

$$A = \alpha \qquad \text{for } \alpha < 1$$

where

$$\alpha = [\text{diameter (sample)/diameter (beam)}]\cos(\theta_1) \qquad [3].$$

Acetonitrile was used as the test medium for several reasons: it has been studied in earlier SNIFTIRS experiments[13], bulk phase IR optical constants are available[14], and it is currently being used as a polar solvent in this laboratory. Only the mid-IR region associated with the nitrile C ≡ N stretching mode was modelled since this mode is expected to be the one most affected by the electrode surface. One should note that experimental spectra contain less

pronounced features arising from several other sources. The Fermi resonance mode at 2292 cm^{-1} for CH_3CN has been shown to be shifted to higher wavenumbers upon coordination with alkali metal cations[15,16] and can be expected to show potential dependent behavior upon adsorption. Also the concentration of acetonitrile coordinated to cations in the double layer can be expected to change with electrode potential. Although the IR absorption band intensities have been estimated to be an order of magnitude smaller than similar contributions from adsorbed species[11,17] such bands will affect the measured IRRA spectrum.

RESULTS AND DISCUSSION

All of the simulated $-\Delta R/R$ curves presented here involve the ratio of the reflectivity for stratified media containing a hypothetical adsorbed layer to the reflectivity for a stratified media containing no adsorbed layer. From the molar volume of pure acetonitrile, a thickness of 0.5 nm is estimated for the the adsorbed monolayer used in the sample case. The thicknesses of the bulk electrolyte layers used were in the range of 4 to 8 μm. These are typical for thin-layer IR spectroelectrochemical cells described in the literature.[1,2,4,5]

Figure 2 compares the $-\Delta R/R$ spectra for three different hypothetical interfacial IRRAS experiments, the initial phase being air and the angle of incidence, $\theta_1 = 60°$. The optical constants for CH_3CN_{ads} were estimated from IR measurements of acetonitrile electrolyte solutions in our laboratory and from SNIFTIRS data.[13] The other optical constants have been taken from the appropriate references and are shown in Table 1. Table 1 also lists the assumed layer compositions and thicknesses for the $-\Delta R/R$ spectra shown in Figure 2.

As can be expected, the SNR is best for the case when there is no absorbing second medium (Figure 2a) and decreases as the absorption coefficient of that medium increases, even though the absorption by the second layer is not measured (Figure 2b). Figure 2c shows the effect of a bulk medium absorption band having a peak position in the vicinity of the same mode associated with the adsorbate layer. It is interesting to note that no dispersion effects are seen in this case; that is, the peak position for the adsorbed CH_3CN is not shifted nor is the band shape distorted due to the proximity of the bulk solvent CN stretching mode.

The comparison in Figure 2 should be refined to include the necessary constraints of a broad band spectrometer, a thin bulk electrolyte layer and an IR window. One of the most important parameters of the IRRAS experiment is the angle of incidence of the IR radiation used to probe the sample. Determining how each of these constraints effects the angle at which the $-\Delta R/R$ signal is maximized helps in optimizing the sampling optics.

The absorption of reflected parallel-polarized IR radiation, from a transparent initial phase, by surface species with dipole moments oriented normal to the reflecting metallic surface increases as a function of the incident angle. Greenler[22] has developed a treatment for this enhancement, showing a maximum effect as the angle of incidence approaches 90°. Despite the fact that Greenler considered the initial semi-infinite phase to be air, this work is often cited, without qualification, with respect to the surface sensitivity of EMIRS and SNIFTIRS experiments.

The optimum angle of incidence for any IRRAS experiment depends on the angular divergence and the beam diameter of the incident radiation. Figure 3 shows how the peak $-\Delta R/R$ position depends on the angle of incidence for the Greenler or gas/solid interfacial experiment. Figure 3a reproduces the idealized case with no angular divergence and a point beam diameter, Figure 3b shows the effect of a focussed beam, and the more realistic situation with both a finite beam size and angular divergence is shown in Figure 3c. On comparing Figures 3a and 3b, one can see the effects of focussed optics. An angular divergence of ±6° (~f/5 optics) reduces the ideal maximum $-\Delta R/R$ value and shifts its position to less grazing angles. Figure 3c shows the effect of a finite beam size, namely, for a 1 cm diameter IR beam on a 2.54 cm diameter sample. The SNR decreases substantially as $\cos(\theta_1)$ becomes small. The faster the spectrometer optics, the more severe the broadening and reduction of the $-\Delta R/R$ peak becomes. As grazing angles are approached, the beam-to-sample ratio should be smaller than the cosine of the incident angle in order to maximize light reaching the sample surface.

Real electrochemical conditions also include the presence of an IR transparent window. Figures 4 and 5 show the $-\Delta R/R$ peak for adsorbed CH_3CN as a function of incident angle for

five different initial phases. The complex dielectric constants used at a frequency of 2350 cm^{-1}, are listed in Table II. In order to identify the effect of a poorly defined electrolyte layer, that is, a wedge-shaped layer or a layer of varying thickness, the curves were calculated for a single thickness of 6 μm (Figure 4) and for an unweighted average of five bulk electrolyte layers with integral thicknesses in the range 4 to 8 μm (Figure 5).

When the initial phase is air, the $-\Delta R/R$ against θ_1 curves are strongly dependent on the thickness of the electrolyte overlayer. This can be seen from the large difference between the averaged and unaveraged 6 μm curves for air in Figures 4a and 5a. The difference between the averaged and unaveraged curves diminishes as the refractive index of the initial phase becomes greater than that of the electrolyte overlayer. The largest difference in refractive indices occurs for a Ge window and, as shown in Figures 4e and 5e, the effect of averaging over a range of electrolyte thicknesses becomes quite small.

Figures 4 and 5 demonstrate that the presence of a window with a refractive index greater than that of the bulk electrolyte (the usual case) tends to average out electrolyte layer thickness effects. These two figures show $-\Delta R/R$ maxima at incident angles near the critical angle for the window/solvent interface. The $-\Delta R/R$ peak value for the CaF_2 window is 4.7 times that for the case with no IR window, while that for the Ge window is 2.1 times as large as the hypothetical windowless case. Such an enhancement of the parallel polarized electric field strength at the adsorbate layer could be due to the coupling of surface plasmon polaritons (SPP) at the metal surface with the evanescent electromagnetic field arising from totally reflected IR radiation present in the window.[23]

Pettinger *et al.*[24] have calculated the enhanced mean squared electric field strength at the electrode surface for a Kretchmann ATR spectroelectrochemical cell, using classical optics. Although the optical system involved a silver electrode, aqueous electrolyte and visible light, the resultant 150 fold enhancement would not be unreasonable in the IR experiments modelled here. At the metal surface the component of the electric field polarized parallel to the plane of incidence can be enhanced relative to the incident field either by constructive interference as a

transverse standing wave or by SPP excitation due to the ATR-produced evanescent electric field. In a SNIFTIRS or EMIRS experiment either mechanism is possible.

Originally,[1] the *in situ* experiments were considered IRRAS techniques, involving the Greenler-type enhancement, where the mean square field strengths are greatest at near grazing angles. The presence of the optically more dense IR window means that, in order to arrive at grazing angles at the electrolyte/electrode interface, the angle of incidence at the window/electrolyte interface must approach the critical angle. Enhancement due to SPP excitation occurs at incident angle values slightly greater than the critical angle. In an electrochemical experiment, uncertainty in the electrolyte layer thickness, angular divergence and a finite beam diameter mean that both enhancement mechanisms could be operative.

Figure 6 shows the correlation between the critical angle (θ_c) of the window/electrolyte interface with the incident angle of maximum intensity for the CH_3CN_{ad} absorption band as a function of refractive index. The calculated curves all show a maximum intensity at an angle a few degrees greater than the critical angle. Experimental work using ATR single reflection crystals[5] has shown a similar trend. Osawa and co-workers measured SPP absorption resonances at angles a few degrees higher than the critical angle. Their experimental configuration precluded any reflection-absorption or Greenler-type enhancement, suggesting that an SPP mechanism accounts exclusively for the simulated *in situ* spectroscopic measurement. However, in the experiments modelled here, the actual $-\Delta R/R$ value represents an average over $\pm 6°$ and ± 2 μm which includes angles below the critical angle and thicknesses different from the resonance value. This means that some contribution from reflection-absorption enhancement is likely, and also that separating the net effects, for the two different phenomena, under experimental conditions is not possible.[25]

Another mechanism which allows for greater absorption by the adsorbate layer is that of optical cavity formation.[26] With the appropriate incident angle, electrolyte layer thickness, window optical constant and IR wavelength, radiation can be most efficiently coupled in and out of the adsorbate layer via constructive interference of multiple reflections. As Roe *et al.*[6]

demonstrated for a collimated laser source with micrometer controlled electrolyte thickness and good parallelism, an optical cavity can be constructed to minimize overall absorption losses and maximize attenuation due to an adsorbate layer. However, it is expected that contributions from this mechanism for broadband, focussing, IR spectrometers is small.

Not only does the optimum incident angle depend on the critical angle but so does the maximum absorption. Figure 7 shows the intensity maxima for the CH_3CN_{ad} absorption as a function of $\cos(\theta_C)$. The relationship is linear and shows an increasing absorption for increasing critical angle. The physical significance of this relationship is that the mean square electric field strength at the adsorbate layer is strongly dependent on the window/electrolyte solution interface. The optical constants of the two media rather than the electrolyte layer thickness or angular divergence determine the signal strength of the adsorbed species for the *in situ* experiment.

Knowing the optimum θ_1 for a given window material, the $-\Delta R/R$ spectra analogous to Figure 1c can now be calculated. The initial phase in these simulations is the IR window material and the angle of incidence is the angle showing the largest $-\Delta R/R$ value from Figure 6. These optimized simulated spectra are shown in Figure 8. They result from the unweighted average over five thicknesses (4-8 μm) at each of five angles over a range of ± 6° around the optimum angle. Each of the angle-specific spectra is weighted with Gaussian coefficient and the five spectra averaged to produce one spectrum at each integral thickness. This process was repeated for both the sample and the reference reflectivities, followed by noise addition to the single beam reflectivities and, finally, the $-\Delta R/R$ spectra (Figure 8) were calculated.

The most striking features of these spectra are the peak intensities relative to Figure 1 and the concomitant increase in SNR. The IR window and thin bulk electrolyte layer necessary for the *in situ* experiment, can actually improve sensitivity, if the correct window geometry and material are selected. The maximum $-\Delta R/R$ value is largest for CaF_2, the material with the closest matched refractive index to the electrolyte layer; however, the enhancements for the other materials are also substantial and the angles of incidence much more reasonable.

In the case of CaF_2, the critical angle approaches 90°, and two deleterious effects are seen. Due to the small value of $\cos(\theta_1)$ the SNR is degraded around the spectral regions of high absorption, that is, close to the C≡N stretching mode for both the bulk electrolyte the adsorbate layer. In addition, the bulk phase band shows dispersion distortion effects, the peak position is shifted to lower frequency, and the band is not symmetrical. The SNR is most improved for the window with the highest refractive index, and there is a slight decrease in absorption due to bulk acetonitrile, relative to the same band associated with the adsorbed layer, on increasing the window refractive index.

For comparison, the same conditions used to calculate the spectra in Figure 8 were used to calculate the spectra in Figure 9 except that all incident angles were set to 60 ±6°. Some interesting features result from this comparison. For the CaF_2 case shown in Figure 9a, the incident angle is now well below the critical angle, and the CH_3CN_{ad} peak intensity is reduced from that for the optimized case shown in Figure 8a. The negative going band for bulk CH_3CN is enhanced in Figure 9a relative to that in Figure 8a and shows none of the dispersion distortion effect.

At angles less than the critical angle, the *in situ* experiment does not discriminate between adsorbate and bulk contributions as well as it does for angles slightly greater than the critical angle of the window/bulk electrolyte solution interface. Figures 9b through 9d demonstrate the expected spectra for incident angles well above the critical angle. The net effect is an overall lowering of adsorbate and bulk absorption. This is to be expected as the position dependent evanescent field strength is lower at angles much greater than the critical angle.

In the preceding discussions the IR window has been treated as a semi-infinite initial phase, no attention being directed to the means by which the radiation actually enters the window. Many of the SNIFTIRS and EMIRS experiments reported in the literature are performed using optical flats as the IR window. The advantages to such a simple disc geometry are low cost and ease of use. More and more frequently, researchers are using Dove prism windows (see references 4 and 5). The reflection losses are much lower relative to

optical flats but the cost is approximately an order of magnitude higher. Hemicylindrical windows provide very similar window/bulk electrolyte optics to the Dove prism but also allow to vary the angle of incidence without changing the angle of refraction. All three of these IR window geometries are schematically shown in Figure 10.

Because of the high refractive indices involved, it is impossible to achieve the optimum incident angle at the IR window/bulk electrolyte interface (θ_2) using an optical flat. Assuming an incident angle at the air/IR window interface of 80°, θ_2 values along with optimum values calculated with the IR window material as the initial phase, are listed in Table 3. For θ_1 equal to 80° and a flat window geometry, θ_3 is equal to 47° regardless of the window material. This angle is much lower than the calculated[22] IRRAS maximum of 88°; thus, the mean square electric field strength enhancement at the adsorbate layer is less than one half of the field strength obtained for a grazing angle of 88°.

Another concern regarding IR windows is the loss of transmitted light intensity due to reflections at interfaces other than the adsorbate/electrode interface. The largest factor in these losses will be that due to reflection at the air/window interface. The square of the transmissivity of p-polarized light at the air/window interface can be used as a first approximation for the actual intensity reaching the sample layer. As Table 3 shows, reflection losses are only substantial in the case of CaF_2, and decrease as the window refractive index increases.

A Dove prism is constructed so that normal incident angles at one of the the two side faces (the air side) result in a particular angle at the bottom face (the electrolyte solution side). Despite the normal angle of incidence, in both the Dove prism window and the hemicylindrical window, there are still reflection losses. The square of transmissivities for a normal angle of incidence are listed in the fourth column of Table 3. The amount of IR light reaching the electrode surface is greater in the case of the two shaped windows relative to the flat window and, in contrast to the flat window case, the transmissivity decreases as the refractive index increases.

Both the hemicylindrical and Dove prism windows act as lenses changing the focal point such that the larger the refractive index, the larger the change. This should be considered when calculating the position of the spectroelectrochemical cell relative to the instrument focal point. For a typical ZnSe Dove prism, the relative change is less than 2.5 mm and the beam spread introduced by not correcting for the window lens effect would not seriously decrease the overall intensity. For a ZnSe hemicylindrical window the focussed beam can be collimated by placing the cell after the instrument focal point a distance determined by the window refractive index and its radius. This distance is much larger than in the previous case, on the order of 20 mm, and the spectroelectrochemical cell assembly should be constructed accordingly.

As a final example, the simulated $-\Delta R/R$ spectra using a flat ZnSe window, at an angle of $60 \pm 6°$, and a hemicylindrical or Dove prism ZnSe window, with $\theta_2 = 36 \pm 6°$, are compared in Figure 11. As with previous examples, an average electrolyte thickness of 6 ± 2 μm was used and noise was injected into the sample and reference reflectivities. Neither Figure 11a nor 11b show any signs of dispersion-distortion effects; in addition, the higher frequency peak due to the adsorbate layer shows a 2 fold increase in intensity for the Dove prism case relative to the optical flat case.

CONCLUSIONS

The presence of an IR window with a refractive index higher than that of the bulk electrolyte solution improves the $-\Delta R/R$ peak intensity for an adsorbate layer relative to the similar experiment with no window. It follows that it is also necessary to consider not only the Greenler or "surface selection rule" mechanism[3,22] but also the coupling of surface plasmons to the infrared evanescent wave, a surface electromagnetic wave (SEW) mechanism[23,25], when discussing the enhancement of the electric field at the metal surface relative to the mean squared incident electric field strength.

The maximum intensity for an IR absorption due to an adsorbate species is achieved with an angle of incidence, in the IR window, a few (1-3) degrees higher than the critical angle for

the IR window/bulk electrolyte solution interface. This numerical determination agrees with the experimentally determined absorption maxima of Osawa *et al.*,[5] in whose experiments only SEW enhancement was possible.

In IR reflection cells the strength of the electric field at the electrode surface is strongly dependent on angle of incidence, and IR window material and geometry. To a much less extent, the field also depends on the angular divergence of the IR beam and the thickness of the bulk electrolyte layer. For the same band due to the adsorbate layer, under differing conditions of IR window material and geometry, the $-\Delta R/R$ intensities differ. Optical conditions, including window material and geometry, must be considered before calculating absolute intensities.

The present work has used classical electromagnetic theory to simulate IRRA spectra for an adsorbed solvent monolayer on a gold surface through a bulk solvent layer. Although the effect of varying electrode potential has not been addressed here, the perturbation of the applied electric field on the optical constants of the adsorbed layer can be empirically determined, using such simulations to fit experimental data. In addition, in the future such an algorithm could be used with experimental data to determine the complex refractive index and the surface concentration of specifically adsorbed molecules. The analytical problem of correlating peak intensities with surface concentrations can be overcome by using such calculations in conjunction with electrochemical capacitance measurements.

ACKNOWLEDGEMENTS

The authors gratefully acknowledge the financial support of the U.S. Office of Naval Research, Washington.

REFERENCES

1) A. Bewick and S. Pons in *Advances in Infrared and Raman Spectroscopy* Vol. 12, R.J.H. Clark and R.E. Hester Eds., Heyden: Philadelphia, 1985, Chapter 1.

2) B. Beden and C. Lamy in *Spectroelectrochemistry*, R.J. Gale Ed.; Plenum Press: New York, 1988, Chapter 5.

3) M.D. Porter, Anal. Chem., **1988**, 60, 1143A.

4) H. Seki, K. Kunimatsu, W.G. Golden, Appl. Spectrosc., **1985**, 39, 437.

5) M. Osawa, M. Kuramitsu, A. Hatta, W. Suetaka and H. Seki, Surf. Sci., **1986**, 175, L787.

6) D.K. Roe, J.K. Sass, D.S. Bethune and A.C. Luntz, J. Electroanal. Chem., **1987**, 216, 293.

7) D.S. Bethune, A.C. Luntz, J.K. Sass and D.K. Roe, Surf. Sci., **1988**, 197, 44.

8) M. Born and E. Wolf *Principles of Optics*; 6th (corrected) Edition, Pergamon Press: Oxford, 1987, Chapter 1.

9) J.D.E. McIntyre in *Advances in Electrochemistry and Electrochemical Engineering*, Vol. 9, R.H Muller Ed.; Wiley & Sons: New York, 1973, Chapter 2.

10) W.N. Hansen, *J.* Opt. Soc. Amer., **1968**, 58, 380.

11) P.W. Faguy, PhD. dissertation, Case Western Reserve University, Cleveland, OH, 1989

12) F. Abeles, Ann. d Physique, **1950**, 5, 611. See also reference 10 and pages 55 - 70 of reference 8.

13) S. Pons, T. Davidson and A. Bewick, J. Electroanal. Chem., **1984**, 160, 63.

14) T.G. Goplen, D.G. Cameron and R.N. Jones, Appl. Spectrosc., **1980**, 34, 657.

15) Z. Kecki and J. Witanowski, Roczniki Chem., **1964**, 38, 691.

16) I.S. Perelygin and M.A. Klimchuk, Russ. J. Phy. Chem., **1973**, 47, 1138.

17) P.W. Faguy, S.McCullough and W.R. Fawcett, The Electrochemical Society Spring Meeting, Los Angeles, May 1989 , Abstract #555.

18) B. Dold and R. Mecke, Optik., **1965**, 22, 435.

19) The complex refractive index was calculated assuming a Lorentzian band at 2350 cm^{-1} with $\gamma = 7.5$ cm^{-1} and a maximum absorption coefficient of 0.1.

20) A.N. Rusk, D. Williams, M.R. Querry, *J.* Opt. Soc. Am., **1971**, 61, 895.

21) The optical constants from reference 14 with $\gamma = 10$ cm^{-1} were used to calculate the complex refractive index.

22) R.G. Greenler, J. Chem. Phys., **1966**, 44, 310.

23) D.M. Kolb in *Surface Polaritons*, V.M. Agranovich and D.L. Mills Eds., North-Holland: Amsterdam, 1982, Chapter 8.

24) B. Pettinger, A. Tadjeddine and D.M. Kolb, Chem. Phys. Lett., **1979**, 66, 544.

25) H. Ishida, Rubber Chemistry and Technology, **1987**, 60, 497.

26) N.J. Harrick and A.F. Turner, Appl. Opt., **1970**, 9, 2111.

Table I. Composition and layer thicknesses used to calculate the IRRAS spectra shown in Figure 1.

SPECTRUM		LAYER	COMPOSITION (references)	THICKNESS (μm)
1a	R_r	1	air	--
		2	air	6.0
		3	gold (18)	--
	R_s	1	air	--
		2	air	5.9995
		3	CH_3CN_{ad} (19)	0.0005
		4	gold	--
1b	R_r	1	air	--
		2	water (20)	6.0
		3	gold	--
	R_s	1	air	--
		2	water	5.9995
		3	CH_3CN_{ad}	0.0005
		4	gold	--
1c	R_r	1	air	--
		2	CH_3CN (21)	6.0
		3	gold	--
	R_s	1	air	--
		2	CH_3CN	5.9995
		3	CH_3CN_{ad}	0.0005
		4	gold	--

Table II. Optical constants used in Figure 3

Material	Complex refractive index at 2350 cm^{-1}
air	1.00
CaF_2	1.41
ZnSe	2.43
Si	3.42
Ge	4.02
CH_3CN	1.36 + 0.0016i
CH_3CN_{ad}	1.29 + 0.1i
Au	2.89 + 26.2i

Table III. Angles of refraction and transmissivities.

	Flat window ($\theta_1 = 80°$)		Dove prism ($\theta_1 = 0°$)	
Material	θ_2	T^2	θ_2	T^2
CaF_2	45°	.584	80°	.998
ZnSe	24	.748	36	.941
Si	17	.895	25	.828
Ge	14	.947	21	.755

FIGURE CAPTIONS

Figure 1. Schematic diagram of an N layer optical system.

Figure 2. Simulated IRRA spectra for 0.5 nm layer of adsorbed CH_3CN with noise injected and no angular divergence or beam attenuation: a) no overlayer, b) 6 μm H_2O overlayer, c) 6 μm bulk CH_3CN overlayer.

Figure 3. $-\Delta R/R$ versus incident angle for $\bar{\nu} = 2350\ cm^{-1}$, adsorbed layer thickness = 0.5 nm: a) with noise injected, b) as in a) with Gaussian averaging for angular divergence, c) as in b) with beam attenuation factor (see equation [2]).

Figure 4. $-\Delta R/R$ versus incident angle for $\bar{\nu} = 2350\ cm^{-1}$, adsorbed layer thickness = 0.5 nm from initial phases a) air, b) CaF_2, c) ZnSe, d) Si and e) Ge. 6 μm thick bulk electrolyte layer.

Figure 5. $-\Delta R/R$ versus incident angle for $\bar{\nu} = 2350\ cm^{-1}$, adsorbed layer thickness = 0.5 nm from initial phases a) air, b) CaF_2, c) ZnSe, d) Si and e) Ge. 6 μm average bulk electrolyte layer thickness, from 4,5,6,7,8 μm calculated reflectivities..

Figure 6. Angle of maximum intensity (filled circles) and critical angle (open triangles) for window/CH_3CN/CH_3CN_{ad}/Au configuration versus window refractive index from data in Figure 5.

Figure 7. Maximum $-\Delta R/R$ values for window/CH_3CN/CH_3CN_{ad}/Au configuration versus the cosine of the window/CH_3CN critical angle from data in figure 5.

Figure 8. Simulated IRRA spectra for 0.5 nm layer of adsorbed CH_3CN through a 6 μm bulk CH_3CN overlayer. a) CaF_2: $\theta_1 = 80°$, b) ZnSe: $\theta_1 = 36°$, c) Si: $\theta_1 = 25°$, d) Ge: $\theta_1 = 21°$. See text for details.

Figure 9. Simulated IRRA spectra for 0.5 nm layer of adsorbed CH_3CN through a 6 μm bulk CH_3CN overlayer, same conditions as in Figure 8 except $\theta_1 = 60°$ for all curves. a) CaF_2, b) ZnSe, c) Si, d) Ge.

Figure 10. Schematic diagram of IR window geometries for *in situ* spectro-electrochemical cells, a) optical flat, b) dove prism, c) hemicylinder.

Figure 11. Simulated IRRA spectra for 0.5 nm layer of adsorbed CH_3CN through a 6 μm bulk CH_3CN overlayer, a) with a ZnSe Dove prism window and an $\theta_1 = 36°$; b) with a Znse flat window 2 mm thick an $\theta = 60°$.

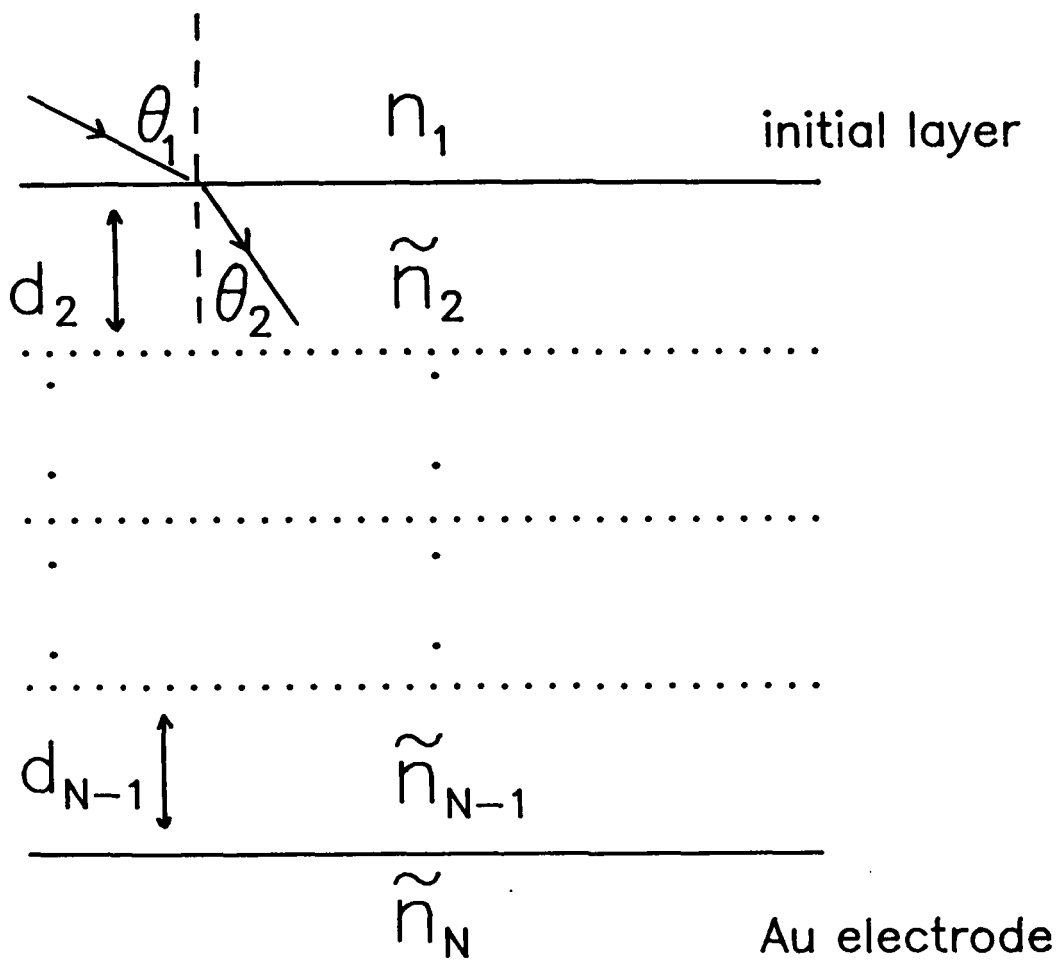

Fig 1, Fagan Fawcett

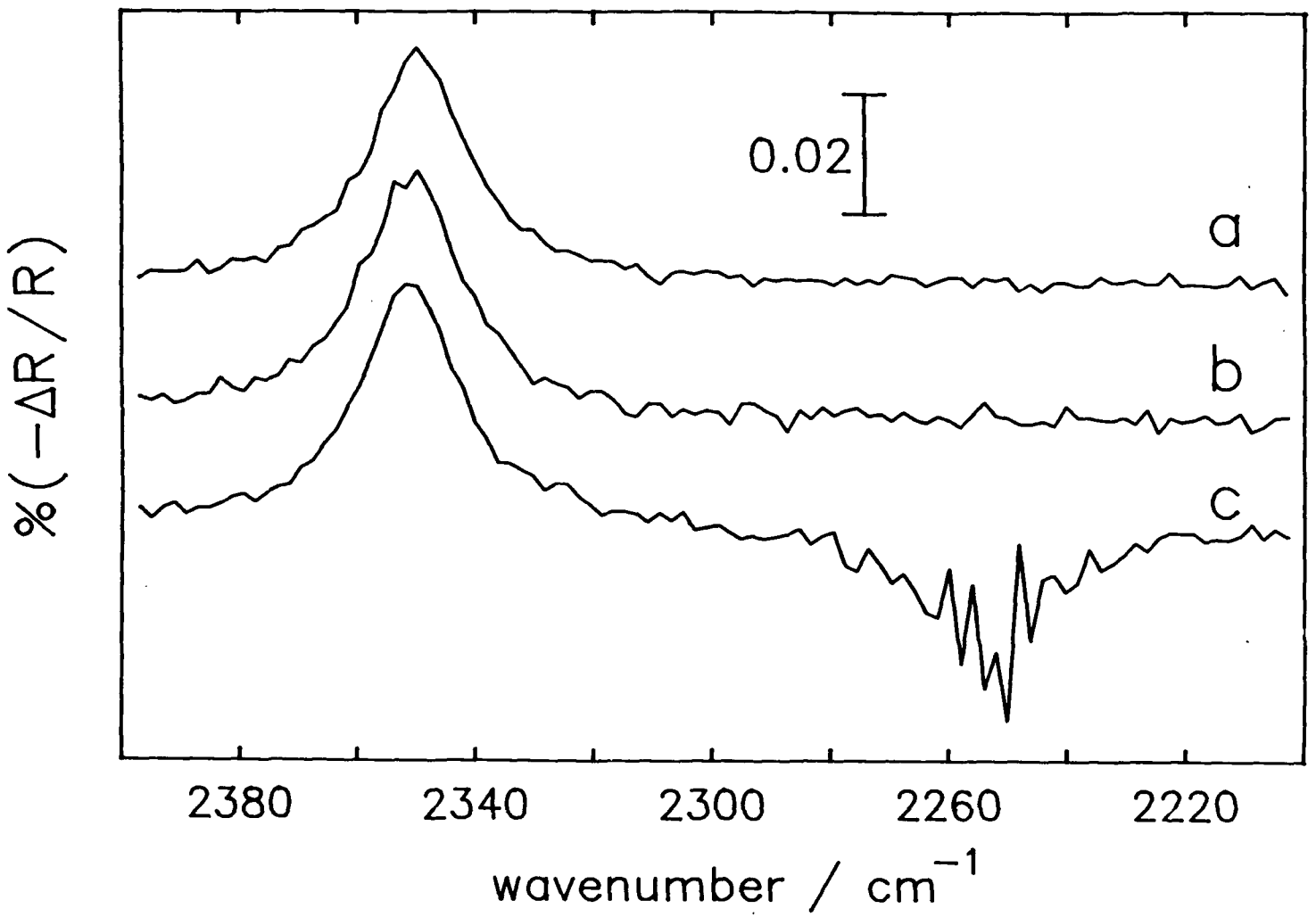

Fig 2
Foguys Fawcett

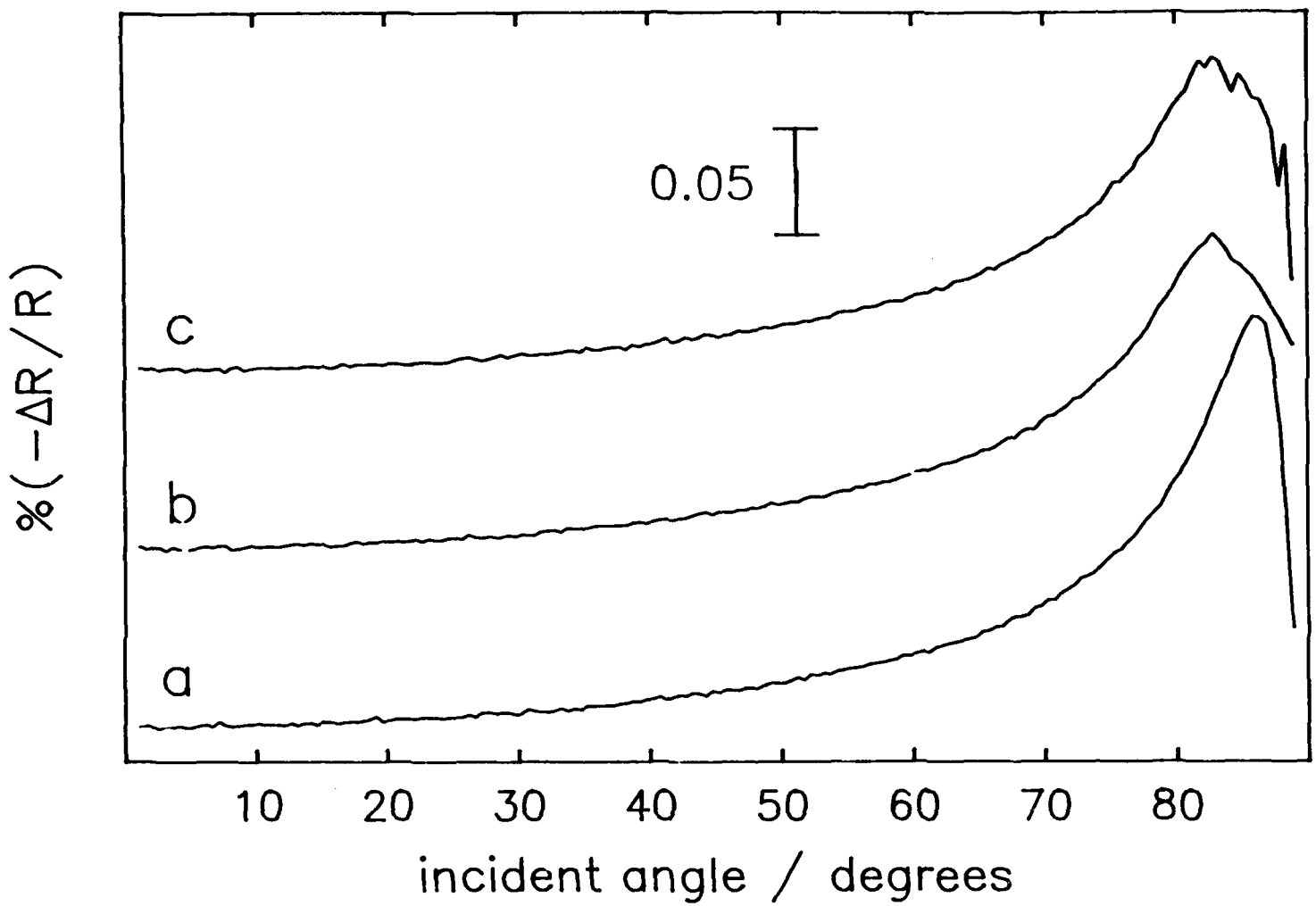

Fig 3
Faguy & Fawcett

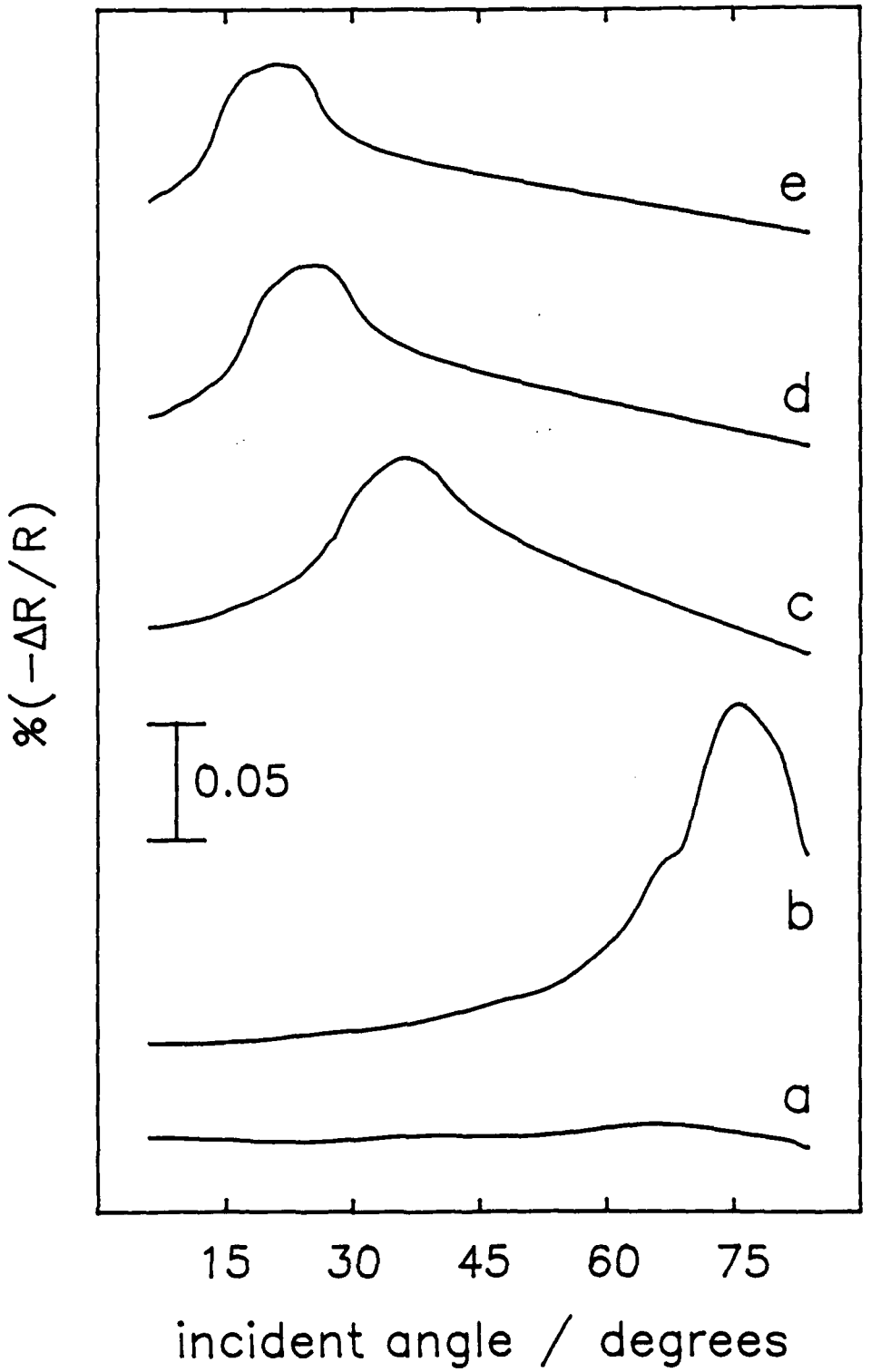

Fig 4.
Faguy & Fawcett

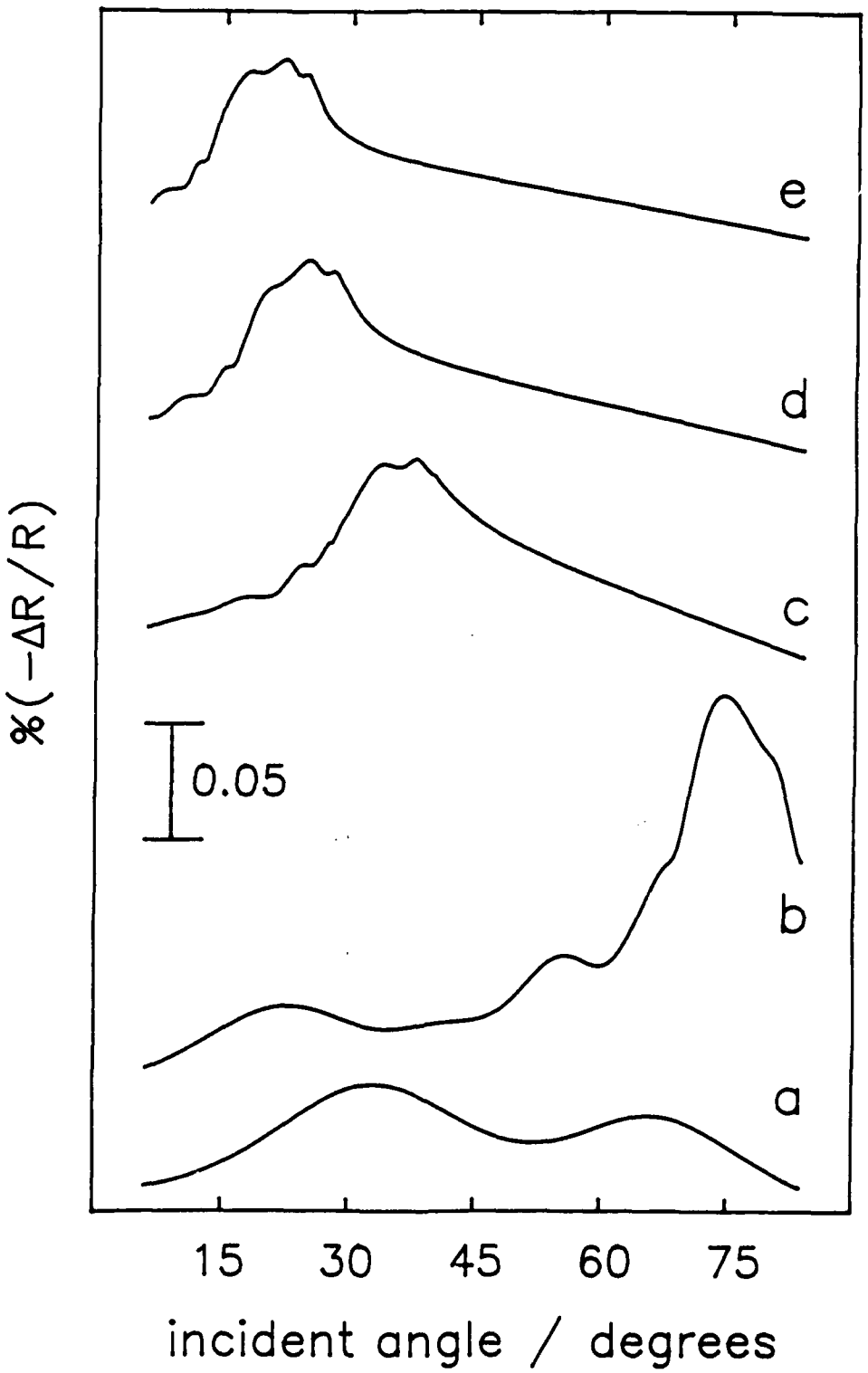

Fig 5
Fagwy & Fawcett

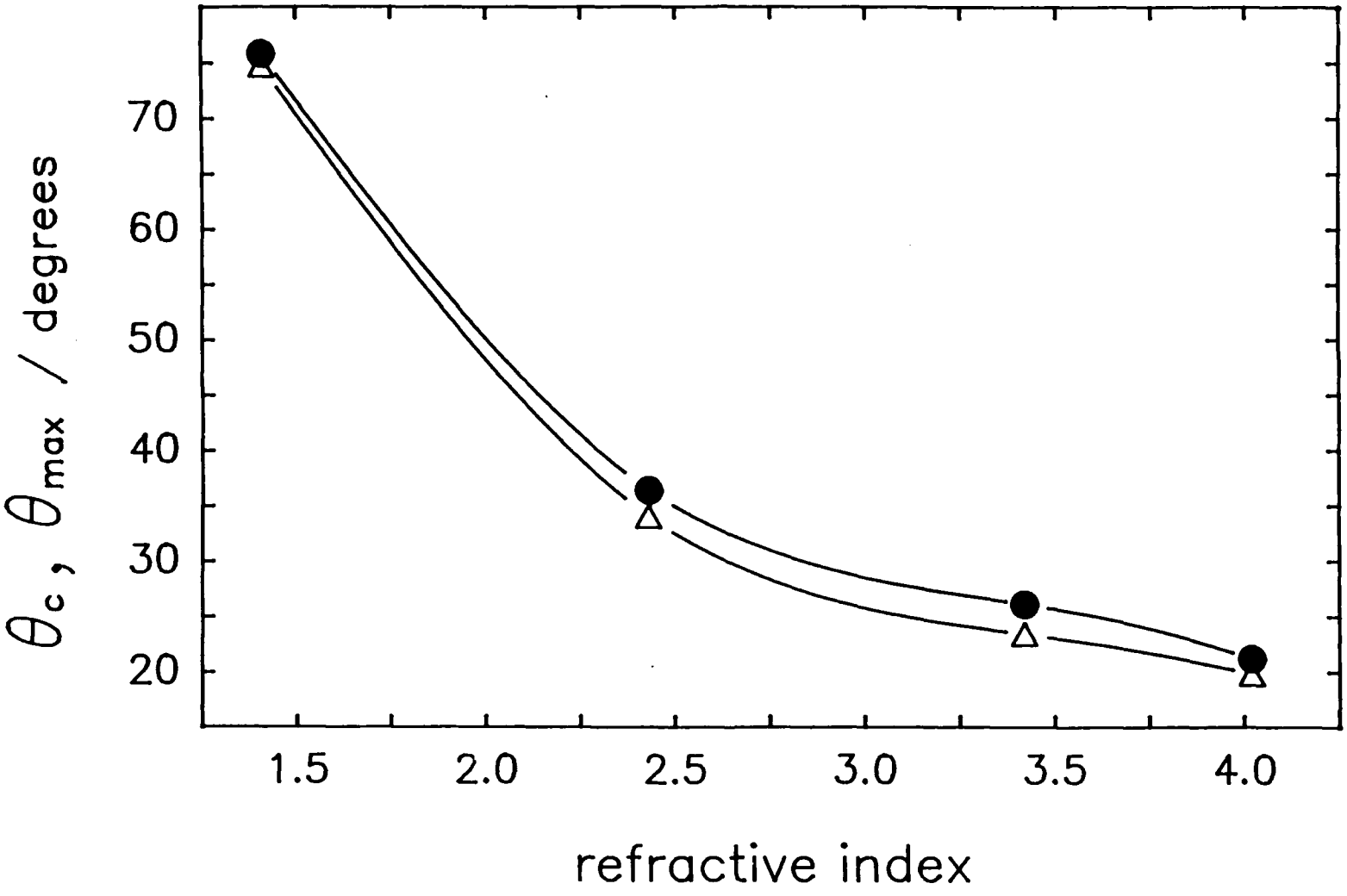

Fig6
Foquy a Fawcett

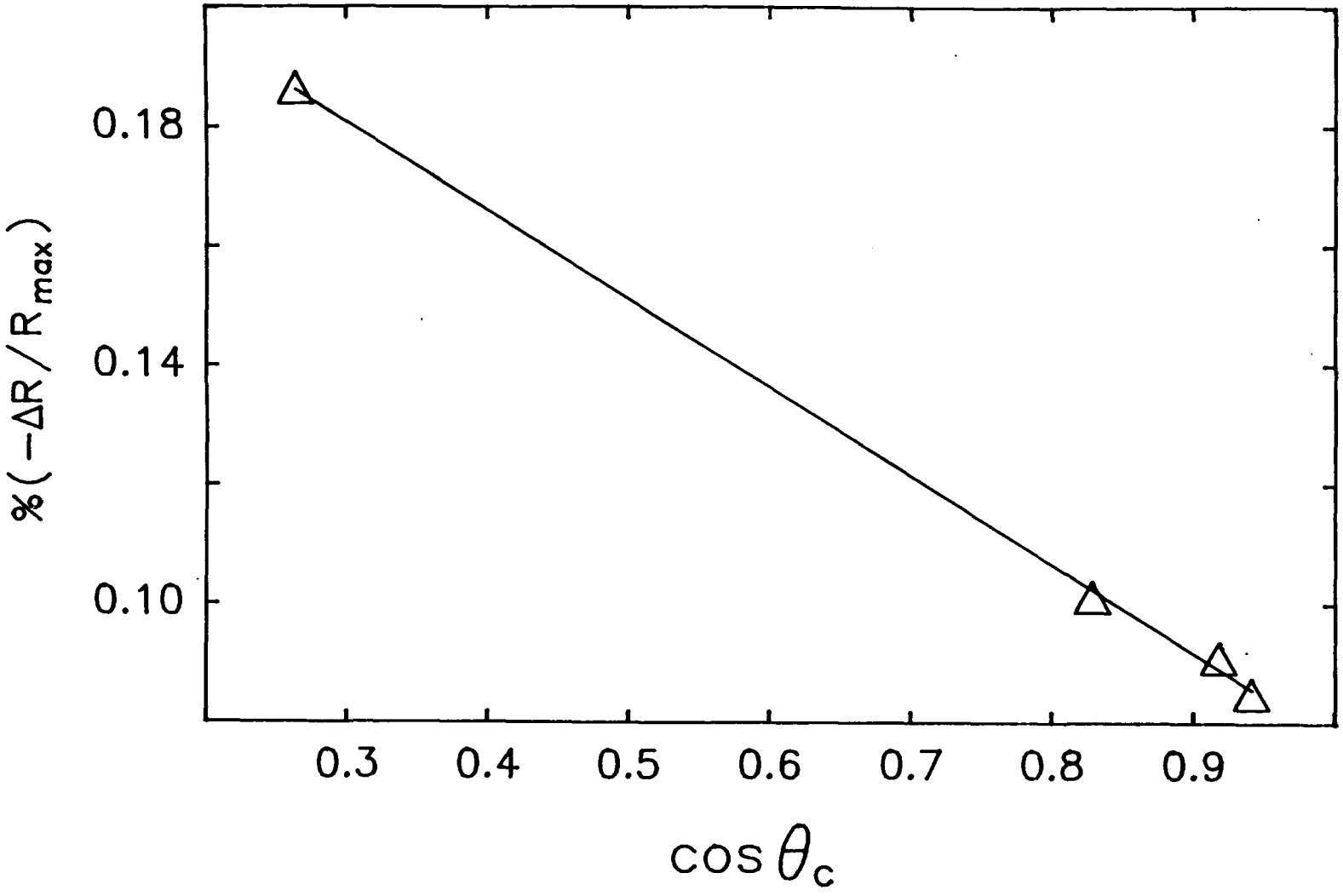

Fig 7
Faquy & Fawcett

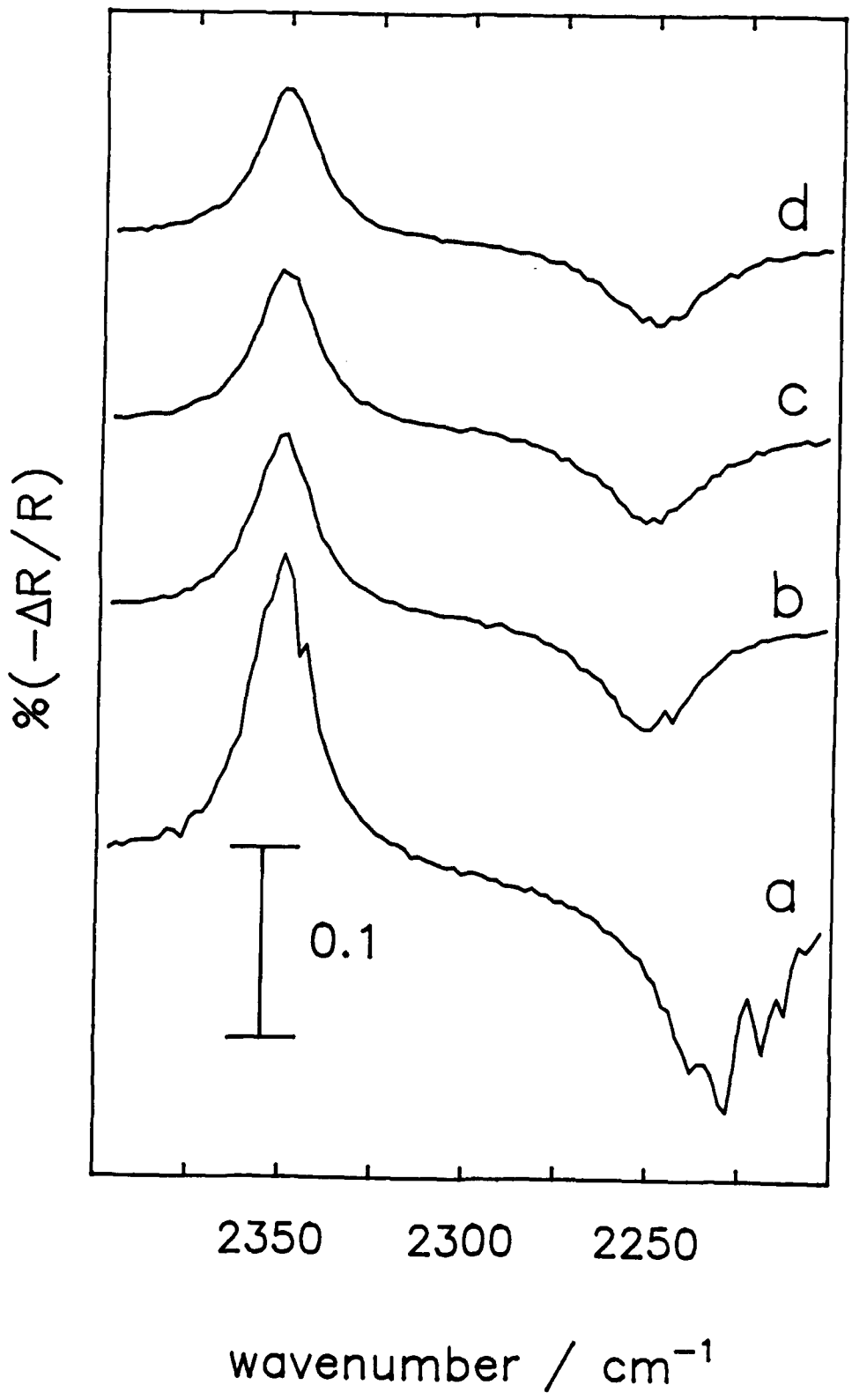

Fig 8

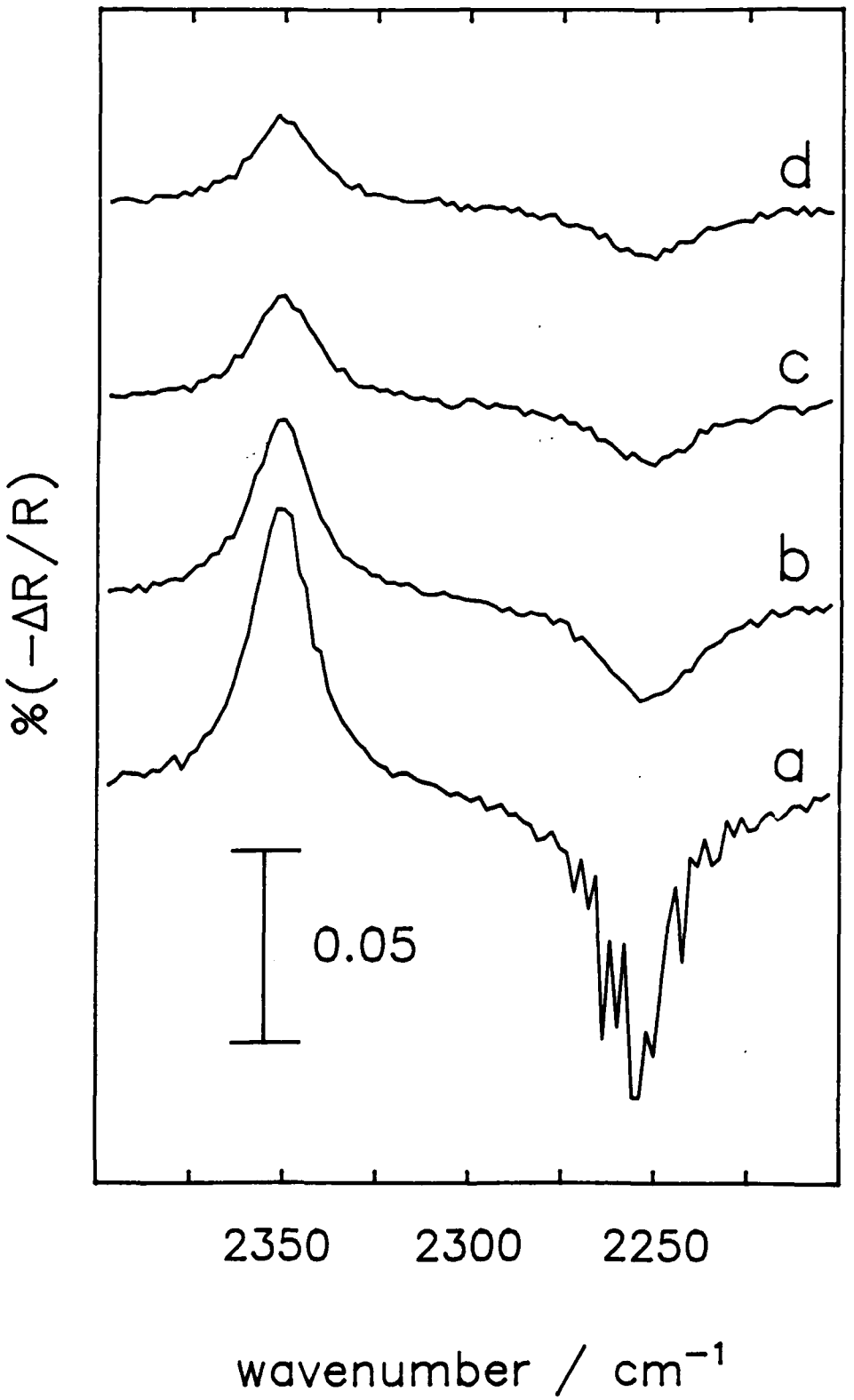

Fig 9
Found Fawcett

Fig 10
Fagny & Fawcett

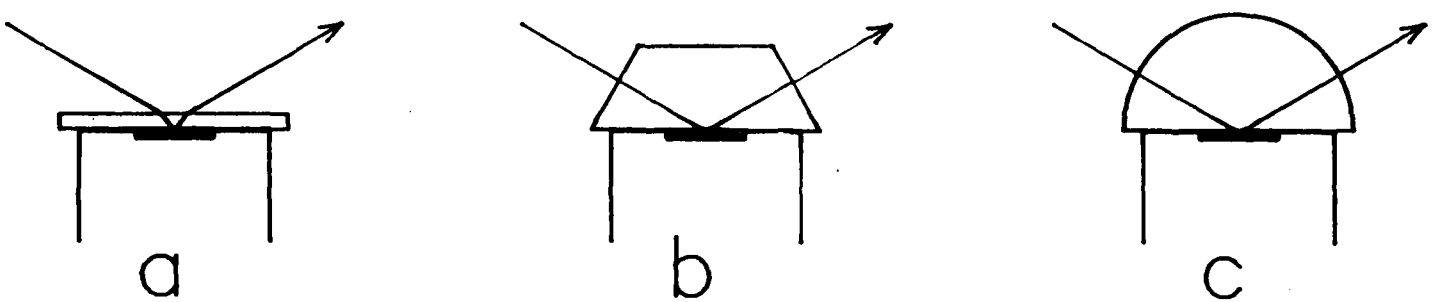

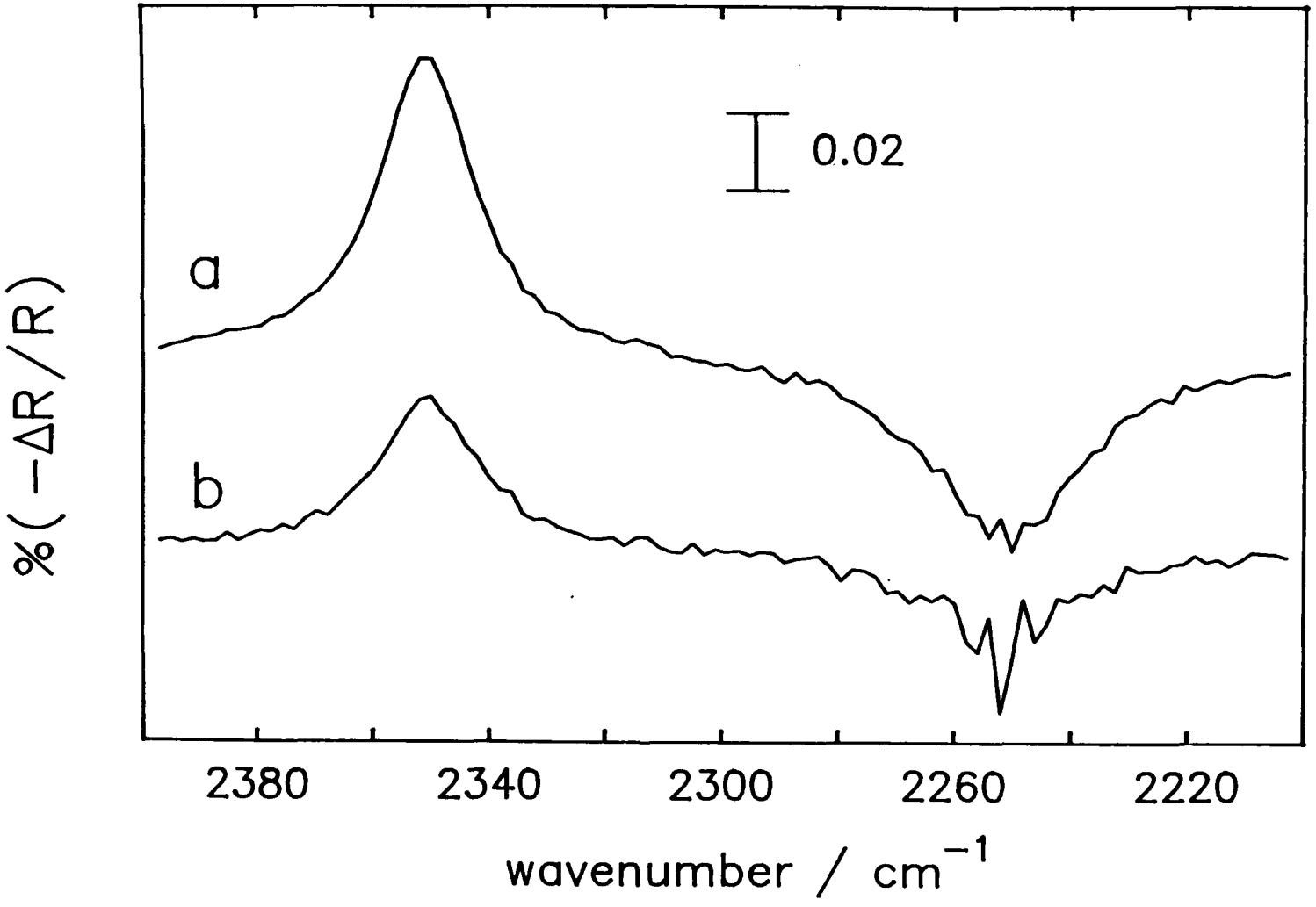

Fig 11.
Faluya Fawcett

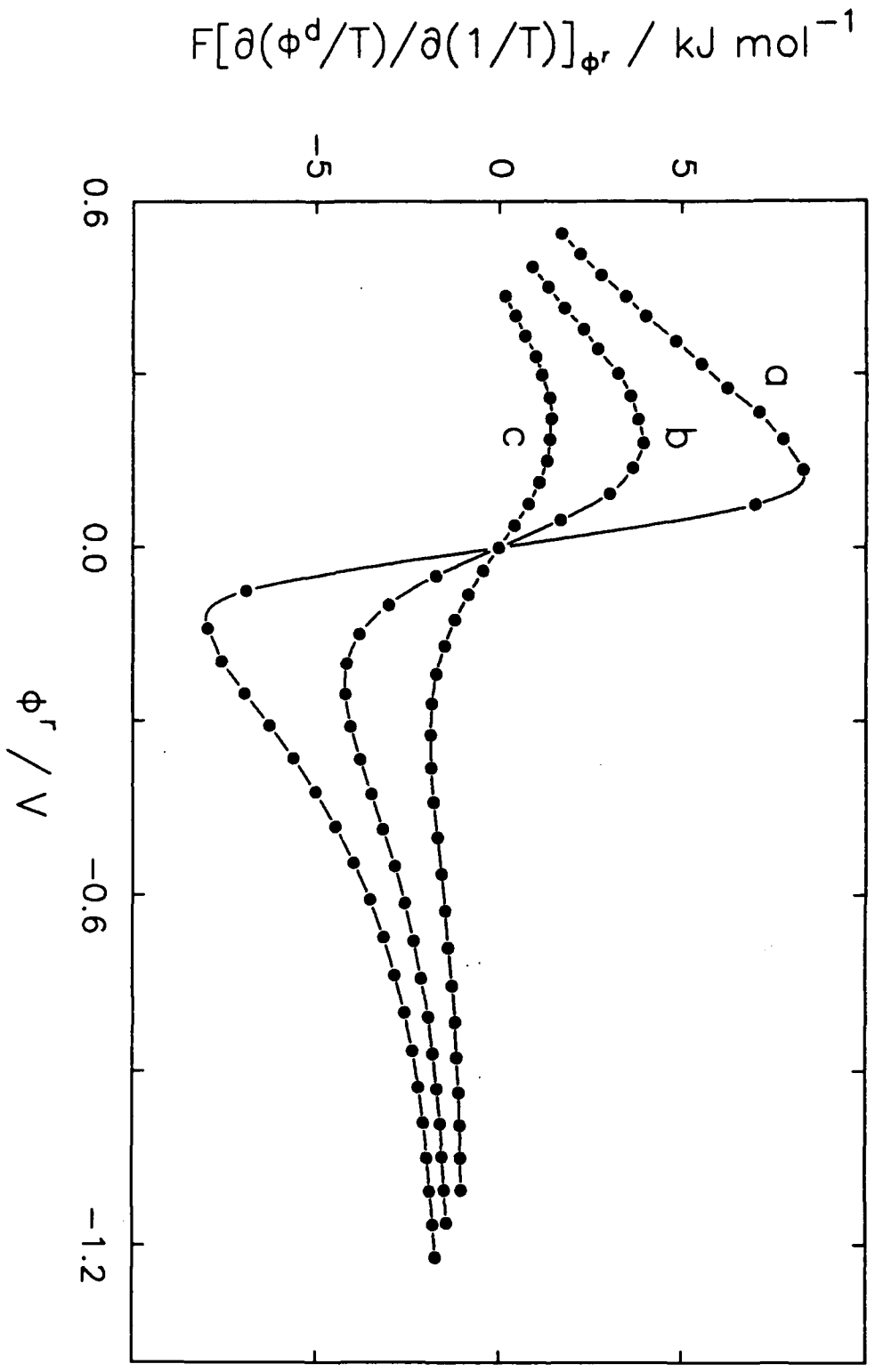
$F[\partial(\phi^d/T)/\partial(1/T)]_{\phi^r}$ / kJ mol^{-1}
−5
0
5
0.6
0.0
−0.6
−1.2
ϕ_r / V
a
b
c

Fig. 1

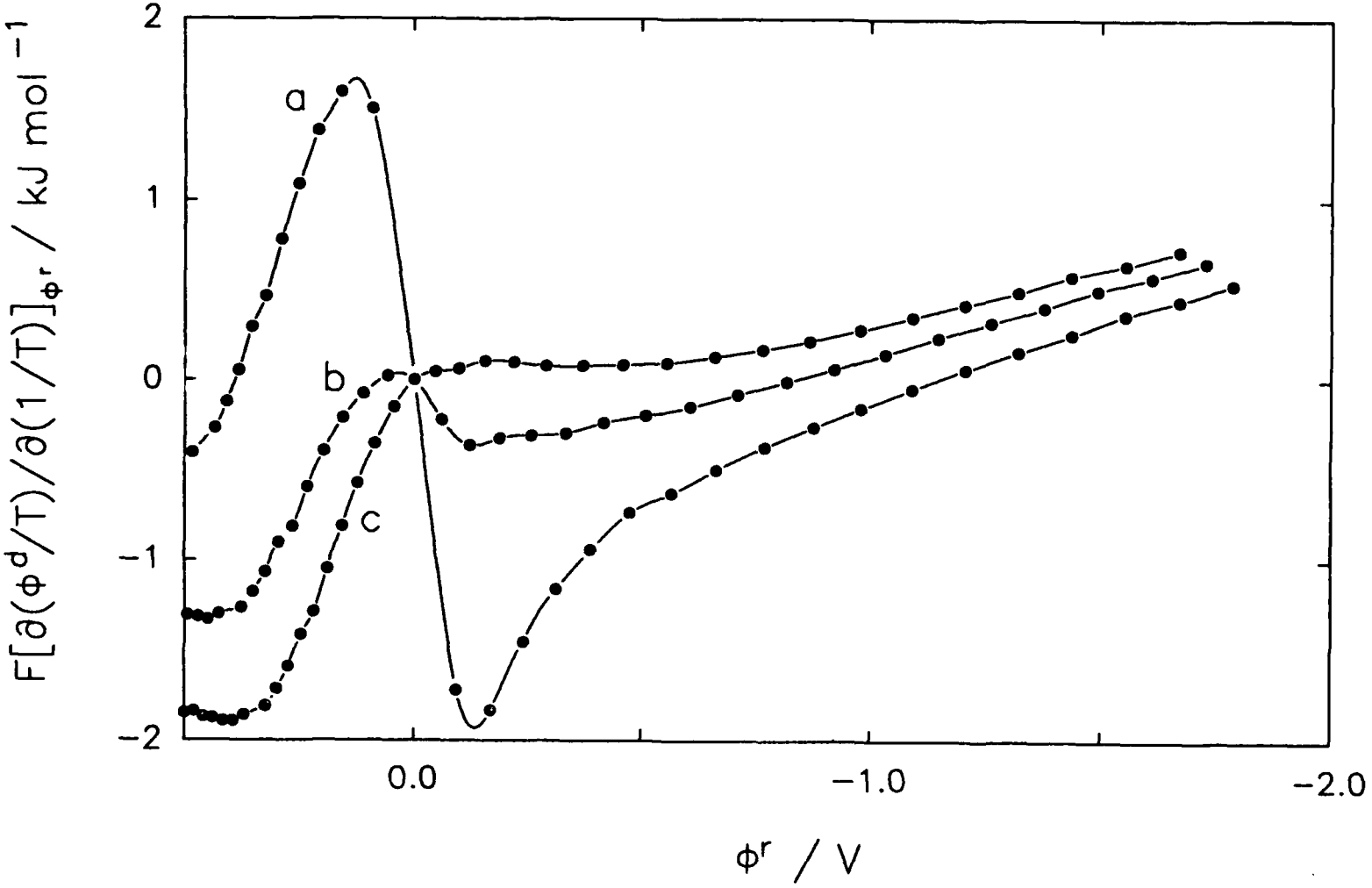
2
1
0
−1
−2
a
b
c
0.0
−1.0
−2.0
$F[\partial(\Phi^d/T)/\partial(1/T)]_{\phi^r}$ / kJ mol^{-1}
ϕ^r / V

Fig. 2

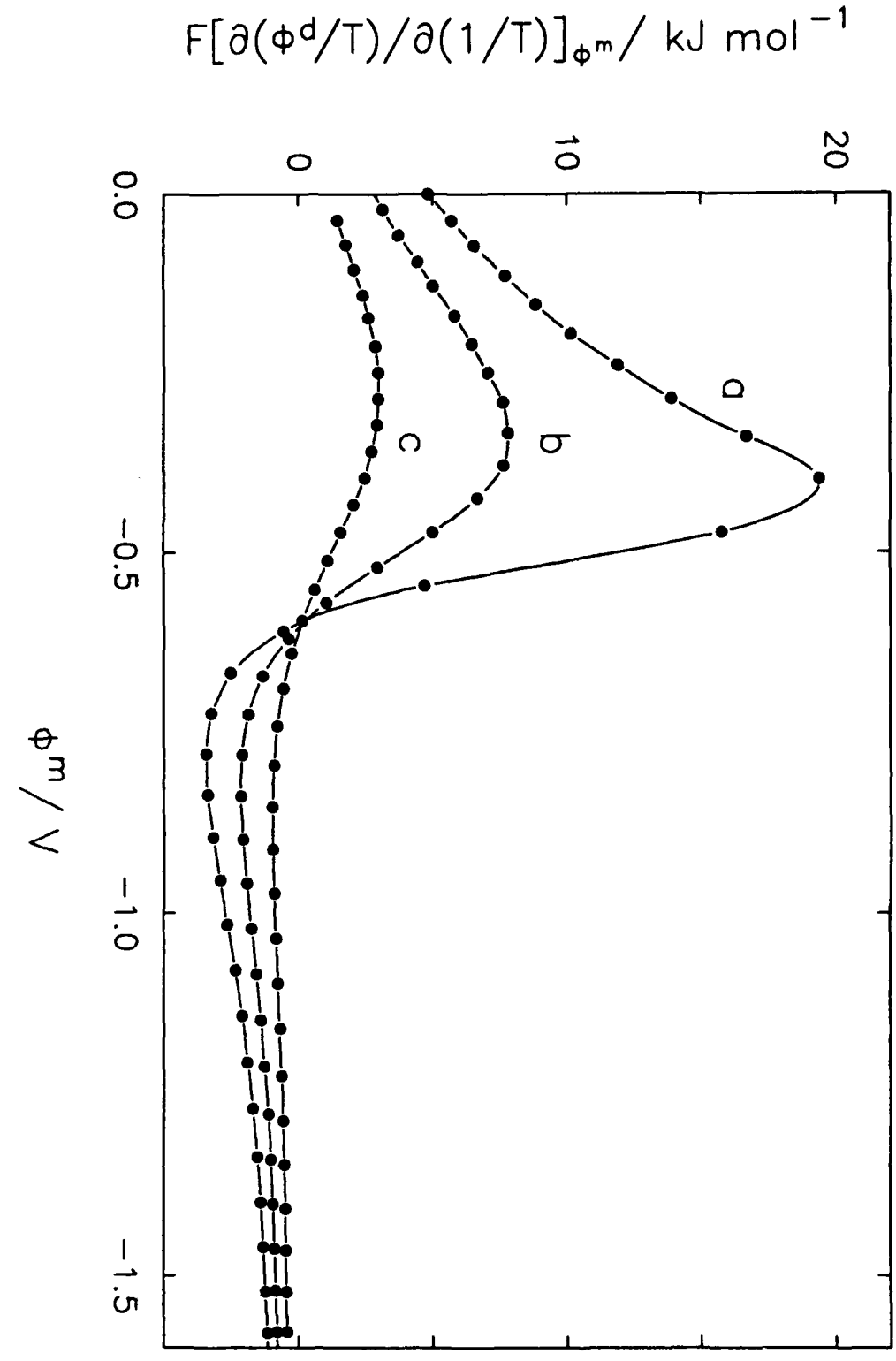

Fig. A1

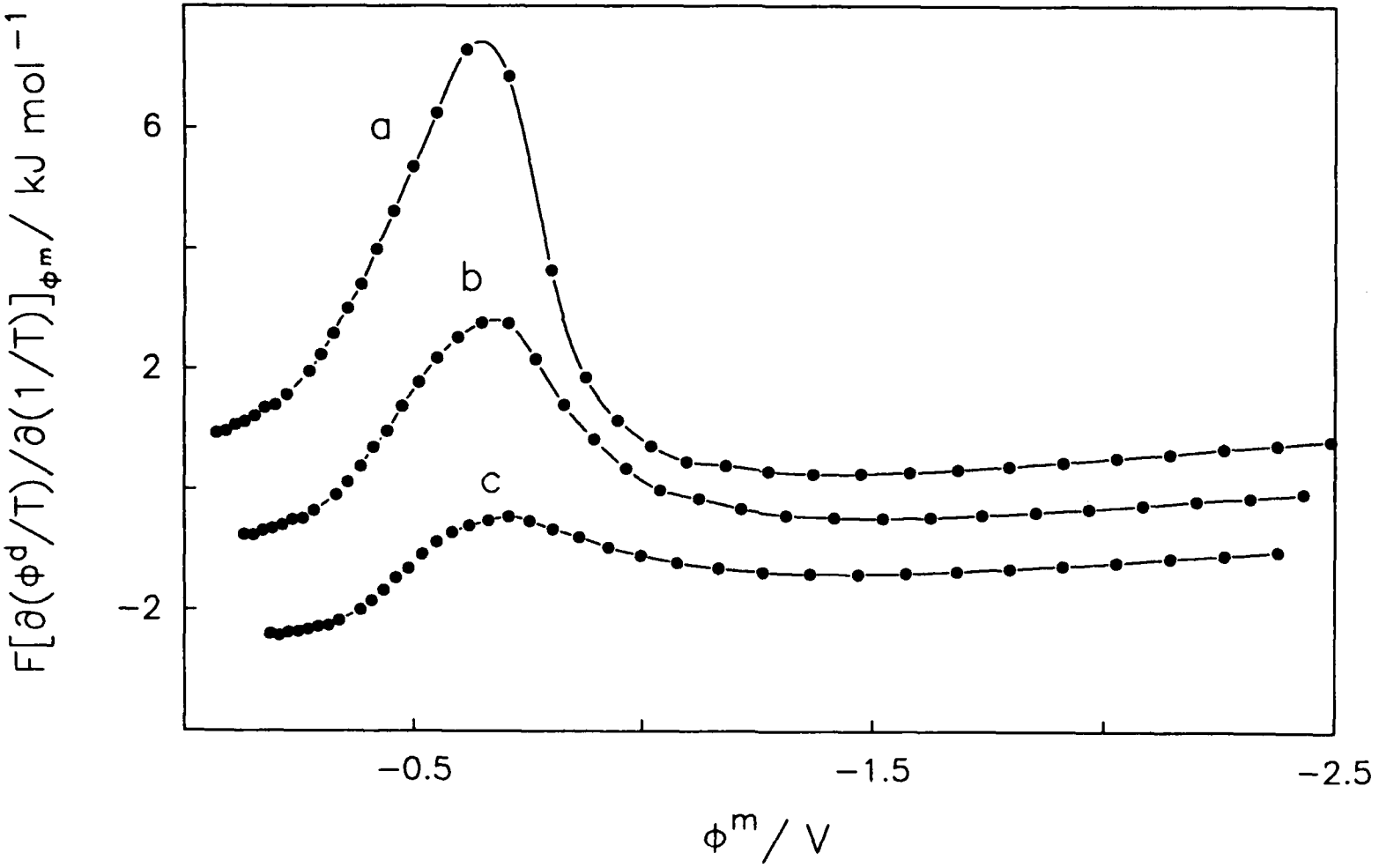

Fig. A2